Supplementary Material for *Dalton Trans.*

Three robust Cd(II) coordination polymers as bifunctional luminescent probes for the efficient detection of pefloxacin and $Cr_2O_7^{2-}$ in water

Xiao-Fei Fan[a], Lianshe Fu[b], Guang-Hua Cui[a*]

[a]*College of Chemical Engineering, Hebei Key Laboratory for Environment Photocatalytic and Electrocatalytic Materials, North China University of Science and Technology, No. 21 Bohai Road, Caofeidian new-city, Tangshan, Hebei, 063210, P. R. China*

[b]*Department of Physics and CICECO-Aveiro Institute of Materials, University of Aveiro, 3810-193 Aveiro, Portugal*

Corresponding author: Guang-Hua Cui

Fax: +86−315−8805462. Tel: +86−315−8805460.

E-mail: tscghua@126.com

Table Titles:

Caption to Figures:

Fig. S20 Reversibility of **3** for the detection of PEF and $Cr_2O_7^{2-}$ ions.

Fig. S21 PXRD patterns of **1** (a), **2** (b), and **3** (c) after sensing analyte.

S1 Synthesis of [Cd(DCTP)(L)(OH)]$_n$ (1)

A mixture comprising $Cd(OAc)_2 \cdot 2H_2O$ (0.2 mmol, 53.30 mg**)**, ligand L (0.1 mmol, 22.63 mg), and H_2DCTP (0.2 mmol, 47.00 mg) were dissolved in 10 mL H_2O. The resulting reaction mixture was transferred into a 25 mL high-pressure reactor lined with polytetrafluoroethylene. Crystallization was induced by heating the reactor to 140°C under self-generated pressure, maintained for 72 hours. After gradual cooling to room temperature at 5°C/h, yellow transparent crystals were isolated by filtration, washed with water and EtOH, and air-dried to yield the product. The achieved yield, calculated with respect to the L ligand, amounts to 56.7%. Anal. Calcd. (%) for $C_{21}H_{17}CdCl_2N_4O_5$ (Mr = 588.68): C, 42.84; H, 2.92; N, 9.52%. Found: C, 43.55; H, 3.02; N, 9.48%. IR (KBr, cm^{-1}): 3487(m), 3118(s), 1580(s), 1551(m), 1525(m), 1371(s),1081(m), 833(m).

S2 Synthesis of [Cd(TBTA)(L)(OH)]$_n$ (2)

The preparation procedure of **2** was similar to **1**, except that H_2TBTA (0.2 mmol, 96.20 mg) is used instead of H_2DCTP. Blocky, Colorless block crystals were obtained after 72 h culture. Yield: 53.2% (based on the L ligand). Anal. Calcd. (%) for $C_{21}H_{15}Br_4CdN_4O_5$ (Mr = 835.41): C, 30.19; H, 1.81; N, 6.71%. Found: C, 29.70; H, 1.95; N, 6.35%. IR (KBr, cm^{-1}): 3287(m), 1600(s), 1528 (m), 1511 (m), 1390(s), 1308(s), 852(m), 741(w).

S3 Synthesis of [Cd(NPHT)(L)(H_2O)]$_n$ (3)

The procedure for the preparation of **3** resembles that of **1**, except that the mixture was replaced by $Cd(OAc)_2 \cdot 2H_2O$ (0.3 mmol, 79.96 mg**)**, ligand L (0.1 mmol, 22.63 mg), H_2DCTP (0.2 mmol, 42.22 mg), H_2O(8 mL), and ethanol (2 mL). Colorless block crystals of **3** were filtered. Yield: 51.2% (based on the L ligand). Anal. Calcd. (%) for $C_{21}H_{19}CdN_5O_7$ (Mr = 565.81): C, 44.58; H, 3.39; N, 12.38%. Found: C, 45.62; H, 4.51; N, 12.18%. IR (KBr, cm^{-1}): 3352(s), 1600(s), 1560(m), 1527(m),

1394(m), 1229(w), 1111(m), 751(s).

S4 Materials and methods

All chemical reagents were procured from commercial sources (Jinan Henghua Sci. & Tec. Co., Ltd) and employed without further purification. Powder X-Ray Diffraction (PXRD) pattern was measured on a Rigaku D/Max−2500PC diffractometer equipped with a 40 kV and 40 mA X-ray tube (λ = 0.15418 nm) on a copper target tube. Fourier Transform Infrared (FTIR) spectra were recorded on a Bruker VERTEX 80 V FTIR spectrophotometer (5000−400 cm^{-1}). Thermal analyses (TGA) were measured by a Netzsch STA449 F1 thermal analyzer from 25 to 800 °C under the air atmosphere protection at a rate of 10 °C·min^{-1}. Ultraviolet–visible (UV−Vis) spectra were recorded on a UV−Vis PuxiT9 ultraviolet-visible spectrophotometer. Elemental analyses (C, H, and N) were measured on a PerkinElmer 240C analyzer. Luminescence spectra were obtained using an Edinburgh Instruments FS5 spectrophotometer.

S5 Computational Details

All calculations on electronic structures were carried out via ORCA 2.8 program.[1] Geometry optimizations was calculated through density functional theory (DFT). A mixed basis sets was chosen for the energy calculation throughout, which corresponds to the double-f basis set with polarization functions 6-31G(d,p) for C, H, N O, Cl and Br, whereas for Cd the pseudo potential LanL2DZ was used.[2,3] The highest occupied molecular orbital (HOMO) and the lowest unoccupied molecular orbital (LUMO) are analyzed using Multiwfn 3.7 program and molecular orbital visualization was analyzed by VMD 1.9.3 program.[4–6] Multiwfn can be freely obtained at http://sobereva.com/multiwfn. VMD can be freely obtained at http://www.ks.uiuc.edu.

S6 X-ray crystallography

The crystal data of **1**−**3** were obtained by Rigaku XtaLab Mini diffractometer equipped with Mo−Kα Radiation at a temperature of 296(2) K (λ = 0.071073 nm). The reflection data is processed using the CrysAlisPro program (version 1.171.38.43). The crystal structure is directly solved by the SHELLXT−2015 program and refined by the full-matrix least square method based on F^2 in the SHELLXT−2018 program. All nonhydrogen atoms are anisotropically refined, the position of hydrogen atoms is geometrically generated, and the ride model is used for isotropic refinement. The main crystallographic data are shown in Table S1. The selected key lengths and key angles are shown in Table S2.

S7 FITR spectra

The IR spectra shows a broad peak at 3487 cm^{-1} for **1**, 3287 cm^{-1} for **2**, and 3352 cm^{-1} for **3**, which are attributed to the O−H tensile stretching mode (Fig. S8).[7] The absence of a strong absorption band for CPs **1**−**3** near 1700 cm^{-1} indicates that the carboxyl group of the organic ligand is completely deprotonated.[8] The asymmetric [V_{as}(COO)] and symmetric [V_s(COO)] stretching vibrations of the carboxylate groups can be observed at different wavenumbers for CPs **1**−**3**: 1580, 1511, 1371 cm^{-1} for **1**, 1600, 1511, 1390 for **2**, and 1600, 1560, 1394 cm^{-1} for **3**. The ΔV values (ΔV = [V_{as} (COO)−V_s(COO)]) demonstrate that the carboxyl groups adopt the monodentate and chelating modes in CPs **1**−**3** (209 and 140 cm^{-1} for **1**, 210 and 121 cm^{-1} for **2**, and 206 and 166 cm^{-1} for **3**).[9] The bands at 1525 cm^{-1} for **1**, 1528 cm^{-1} for **2**, and 1527 cm^{-1} for **3** are caused by the C = N stretching vibrations of the L ligand.[10]

S8 The sensing of antibiotics and metal ions

In order to assess selectivity and sensitivity of CPs **1**−**3** to some common antibiotics, including pefloxacin (PEF), sulfadiazine (SDZ), sulfamethazine (SMZ), sulfamethoxazole (SMX),

metronidazole (MDZ), ornidazole (ORN), ronidazole (RNZ), nitrofurazone (NFZ), nitrofurantoin (NFT), Norfloxacin (NOR), Amoxicillin (AMX), Tetracycline (TC) and Uric acid (UA). 4.0 mg finely ground powders of **1**−**3** were added in 4 mL aqueous solutions, creating the suspension solution under ultrasonic vibration. Further, 200 μL different antibiotics (5×10^{-5} mol·L^{-1}) were slowly dropped into the solution and irradiated ultrasonically again. The blank experiments were also disposed by using the suspension of the samples in water and treating them under the same requirement. The resulting suspensions were promptly used for the measurements of fluorescence recognition. The anti-interference experiments were performed, introducing PEF and other antibiotics into, and aqueous solutions (c:c = 1:1) of **1**−**3** to form suspensions (4 mL).

As for the metal ions, The powder of **1**−**3** (4 mg) was added in aqueous solutions (2 mL) and MeCN (2 mL), which had K_nX (X = $Cr_2O_7^{2-}$, OCN^-, SO_4^{2-}, ClO^{3-}, CO_3^{2-}, H_2PO^{4-}, NO^{3-}, Cl^-, Br^-, I^-, IO_3^-, $P_2O_7^{4-}$, SCN^-, HPO_4^{2-}, BrO_3^-, and HCO_3^-) with a concentration of 5×10^{-4} mol·L^{-1}. Before the luminescence sensing measurement, the mixed suspensions were sonicated for 30 min. The blank experiment was done without adding any metal anions. The CPs **1**−**3** were added to the aqueous suspension containing $Cr_2O_7^{2-}$ and each of the interfering metal ions (0.02 mol·L^{-1}, 2 mL) with the identical concentration in the sensing selective experiments.

References

[1] F. Neese, *Wiley Interdiscip, Rev. Comput. Mol. Sci*.,2012, **2(1)**, 73−78.

[2] P. J. Hay and W. R. Wadt, *J. Chem. Phys*., 1985, **82(1)**, 299−310.

[3] P. J. Hay and W. R. Wadt, *J. Chem. Phys*., 1985, **82(1)**, 270-283.

[4] T. Lu, F. Chen, *J Comput Chem*, 2012, **33(5)**, 580−592.

[5] A. D. Becke, *J. Chem. Phys*., 1992, **96(3)**, 2155−2160.

[6] W. Humphrey, A. Dalke and K. Schulten, *J. Molec. Graphics*, 1996, **14(1)**, 33−38.

[7] J. Zhang, Y. Hu, L. Zhang, J. Zhou and A. Lu, *Nanomicro Lett*, 2023, **15(1)**, 8.

[8] S. Y. Hao, S. X. Hou, K. Van Hecke and G. H. Cui, *Dalton Trans*., 2017, **46(6)**, 1951−1964.

[9] Z. B. Han, X. N. Cheng and X. M. Chen, *Cryst. Growth Des*., 2005, **5(2)**, 695−700.

[10] B. A. Lima, J. de JG Varela Jr, J. Ellena, A. A. Batista, A. B. da Silva and R. S. Correa, *J. Mol. Struct*., 2023, **1282**, 135234.

Table S1. Crystal data and structure refinements for **1**−**3**

CPs	**1**	**2**	**3**
CCDC	2308927	2308928	2308929
Chemical formula	$C_{21}H_{17}CdCl_2N_4O_5$	$C_{21}H_{15}Br_4CdN_4O_5$	$C_{21}H_{19}CdN_5O_7$
Formula weight	588.68	835.41	565.81
Crystal system	triclinic	triclinic	triclinic
Space group	*P*$\bar{1}$	*P*$\bar{1}$	*P*$\bar{1}$
a (nm)	1.022(6)	1.124(5)	1.050(7)
b (nm)	1.077(7)	1.132(5)	1.104(1)
c (nm)	1.162(7)	1.138(3)	1.234(9)
α (°)	117.383(6)	74.967(3)	75.039(7)
β (°)	95.964(5)	75.011(3)	77.438(6)
γ (°)	102.135(5)	67.570(4)	73.334(7)
V (nm^3)	1.081(1)	1.271(1)	1.308(2)
Z	2	2	2
D_{calcd} (g/cm^3)	1.809	2.182	1.436
Absorption coefficient, mm^{-1}	1.301	7.185	0.880
F(000)	586.0	794.0	568.0
Crystal size, mm^3	0.23 × 0.22 × 0.18	0.24 × 0.22 × 0.20	0.26 × 0.22 × 0.20
θ range (°)	2.227~30.537	2.468~30.618	2.246~25.027
Index ranges	$-14 \le h \le 14$, $-15 \le k \le 15$, $-16 \le l \le 16$	$-16 \le h \le 16$, $-16 \le k \le 16$, $-16 \le l \le 16$	$-12 \le h \le 12$, $-13 \le k \le 13$, $-14 \le l \le 14$
Reflections collected	30882	35416	27262
Independent reflections (R_{int})	6274(0.0521)	7446(0.0633)	4600(0.0826)
Data/restraint/parameters	6274/6/301	7446/0/319	4600/1/310
Goodness-of-fit on F^2	1.059	1.048	1.054
Final R_1, wR_2 ($I > 2\sigma(I)$)	0.0381, 0.0976	0.0548, 0.0866	0.0392, 0.1079
Largest diff. peak/hole ($e \cdot nm^{-3}$)	1920/−1290	1120/−970	1400/−990

Table S2. Selected bond lengths (nm) and angles (°) for **1**−**3**

Parameter	Value	Parameter	Value
1			
Cd1−O5	0.244(2)	Cd1−O2	0.249(2)
Cd1−O3	0.222(2)	Cd1−O1	0.230(2)
Cd1−N1	0.229(2)	Cd1−N4(A)	0.231(2)
O5−Cd1−O2	84.83(8)	O3−Cd1−O5	86.83(8)
O3−Cd1−O2	101.10(9)	O3−Cd1−O1	154.66(1)
O3−Cd1−N1	109.93(9)	O3−Cd1−N4(A)	82.04(9)
O1−Cd1−O5	94.80(9)	O1−Cd1−O2	54.06(8)
O1−Cd1−N4(A)	93.38(1)	N1−Cd1−O5	84.50(8)
N1−Cd1−O2	146.47(8)	N1−Cd1−O1	95.38(8)
N1−Cd1−N4(A)	103.44(8)	N4(A)−Cd1−O5	168.02(8)
N4(A)−Cd1−O2	92.92(2)		
2			
Cd1−O1	0.234(3)	Cd1−O3	0.237(3)
Cd1−N1	0.225(3)	Cd1−O2	0.252(4)
Cd1−N4(A)	0.232(4)	Cd1−O5	0.233(4)
O1−Cd1−O2	53.68(1)	O3−Cd1−O1	85.26(1)
O3−Cd1−O2	98.66(1)	O3−Cd1−N4(A)	155.51(1)
O3−Cd1−O5	80.90(1)	N1−Cd1−O1	153.95(1)
N4−Cd1−O3	101.51(1)	N4−Cd1−O2	100.28(1)
N1−Cd1−N4(A)	98.62(1)	N1−Cd1−O5	106.04(1)
N4(A)−Cd1−O1	82.72(1)	N4(A)−Cd1−O2	91.28(1)
N4(A)−Cd1−O5	80.25(1)	O5−Cd1−O1	99.85(1)
O5−Cd1−O2	153.24(1)		
3			
Cd1−O7	0.235(3)	Cd1−O1	0.236(3)
Cd1−O4(A)	0.238(3)	Cd1−O3(A)	0.260(3)
Cd1−N5(B)	0.234(3)	Cd1−N2	0.226(3)
O7−Cd1−O1	77.51(1)	O7−Cd1−O4(A)	83.66(1)
O7−Cd1−O3(A)	79.20(1)	O1−Cd1−O4(A)	161.11(1)
O1−Cd1−O3(A)	124.32(9)	O4(A)−Cd1−O3(A)	51.83(9)
N5(B)−Cd1−O7	98.02(9)	N5(B)−Cd1−O1	91.13(1)
N5(B)−Cd1−O4(A)	90.17(1)	N5(B)−Cd1−O3(A)	141.99(9)
N2−Cd1−O7	169.25(1)	N2−Cd1−O1	107.14(1)
N2−Cd1−O4(A)	91.65(1)	N2−Cd1−O3(A)	90.29(1)
N2−Cd1−N5(B)	91.64(1)		

Symmetry codes for **1**: A: 1−*x*, 2−*y*, 1−*z*; B: −*x*, 1−*y*, −*z*; C: −*x*, 2−*y*, 2−*z*; for **2**: A: 1−*x*, 1−*y*, 1−*z*; B: −*x*, 2−*y*, 1−*z*;

C: 1−*x*, 2−*y*, 2−*z*; for **3**: A: 1−*x*, 1−*y*, 1−*z*; B: 1−*x*, 2−*y*, 1−*z*.

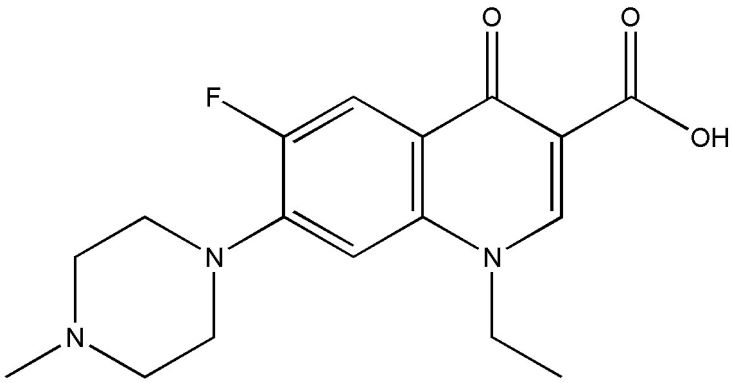

Fig. S1 The chemical structure of PEF.

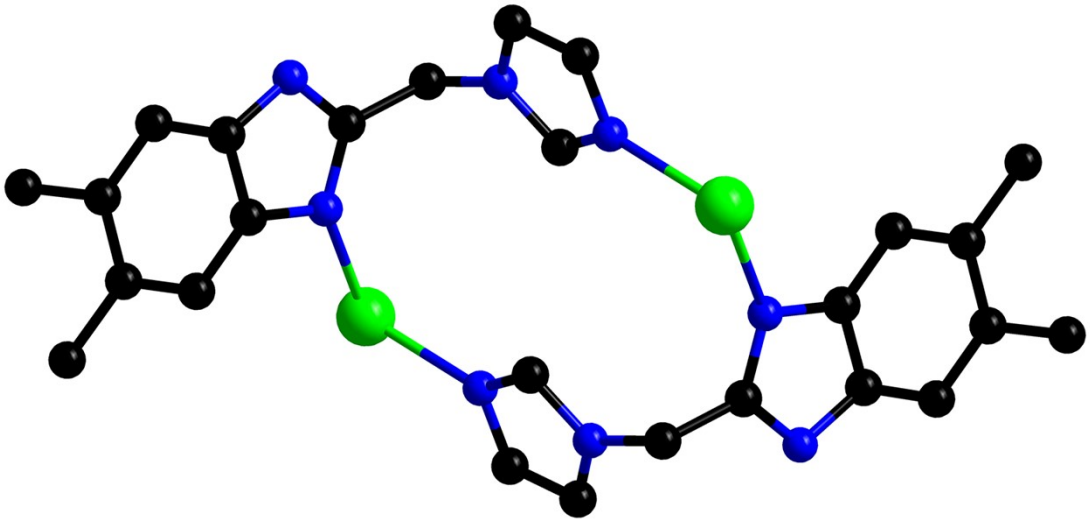

Fig. S2 Metals and L ligands are linked to form a $[Cd_2(L)_2]$ loop.

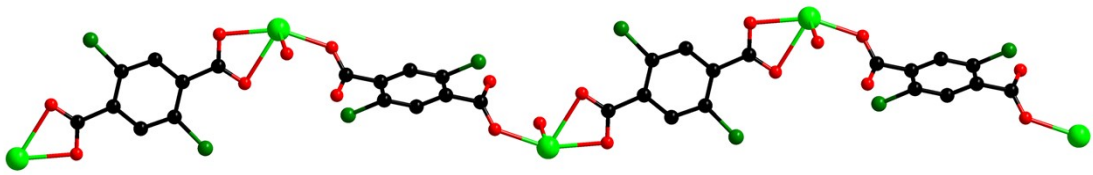

Fig. S3 Metals and $DCTP^{2-}$ ligands connect to form $[Cd(DCTP)]_n$ chains.

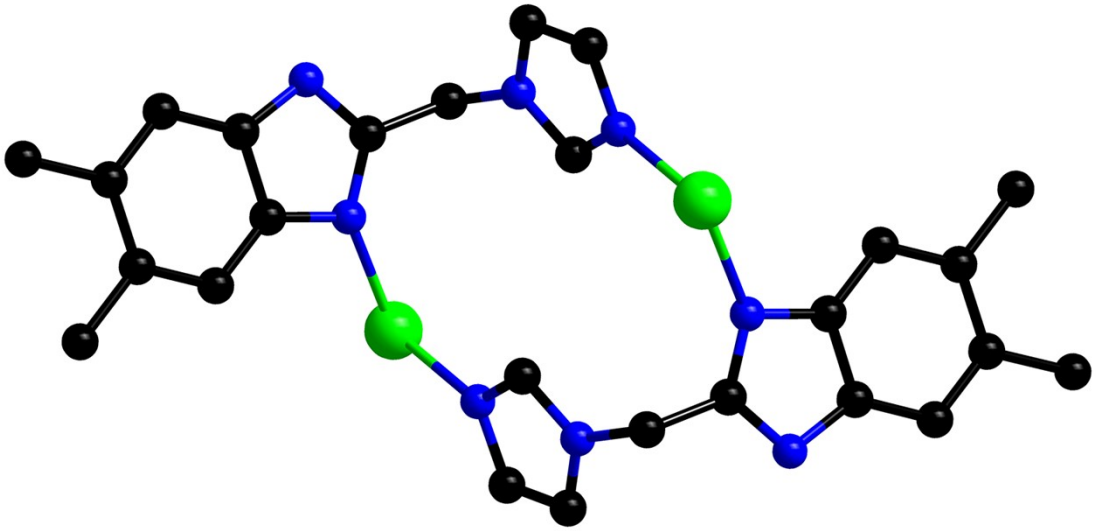

Fig. S4 Metals and L ligands are linked to form a $[Cd_2(L)_2]$ loop.

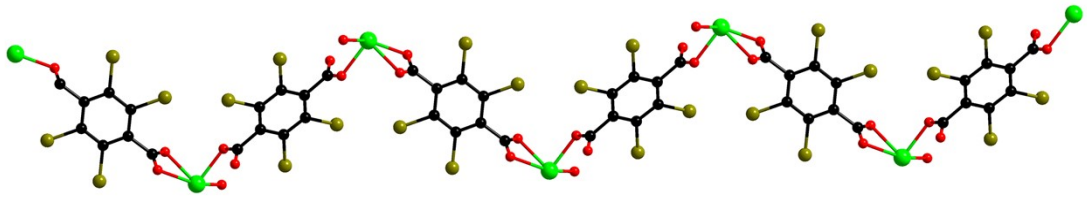

Fig. S5 Metals and $TBTA^{2-}$ ligands are linked to form an infinite chain.

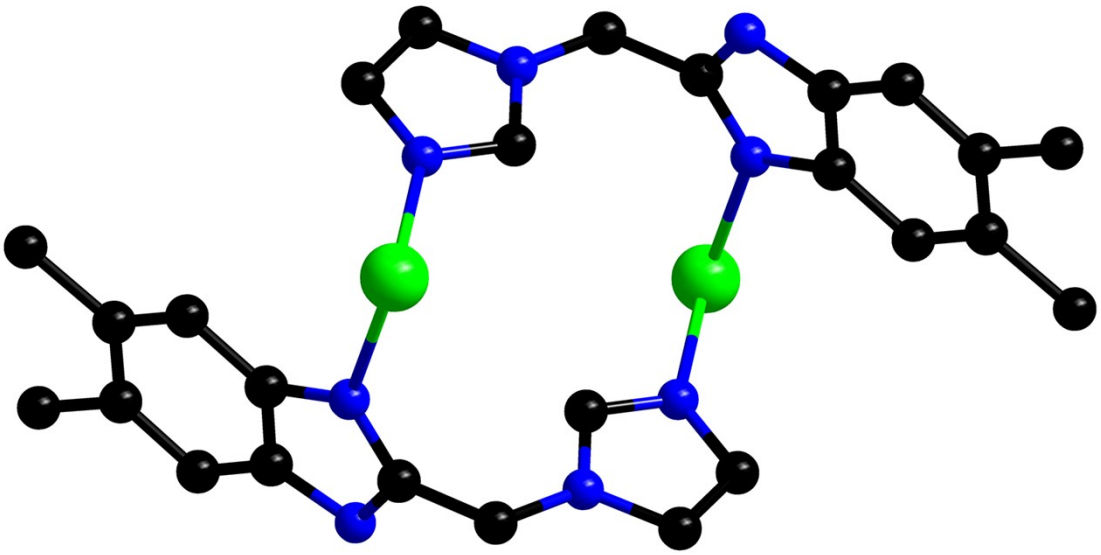

Fig. S6 Metals and L ligands are linked to form a $[Cd_2(L)_2]$ loop.

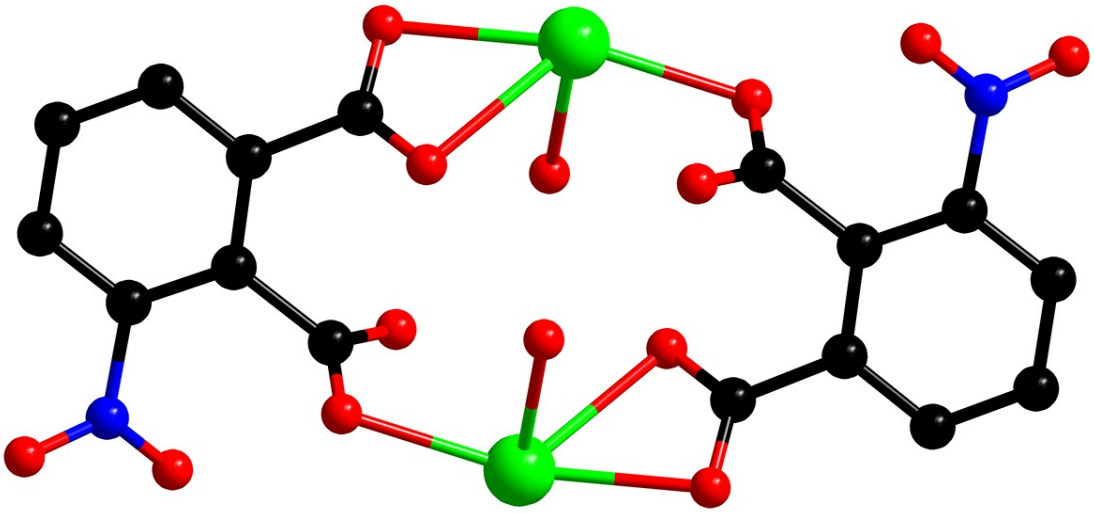

Fig. S7 Metals and $NPHT^{2-}$ ligands are linked to form a $\{Cd_2(NPHT^{2-})_2\}$ loop.

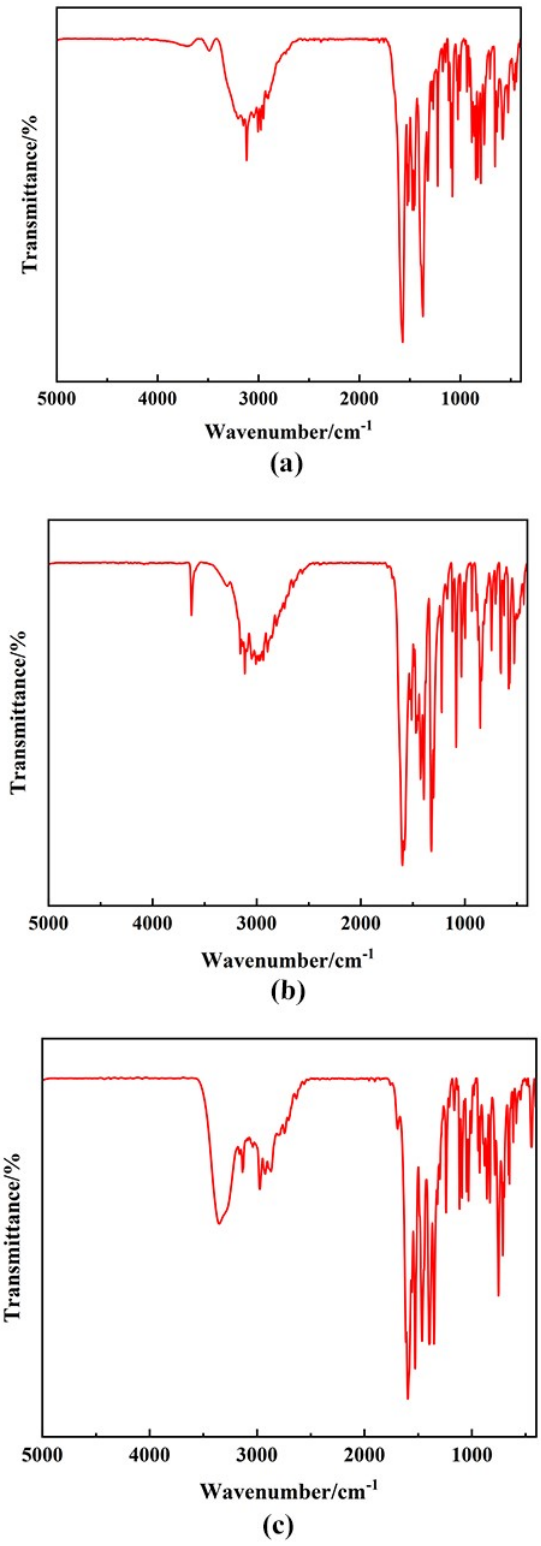

Fig. S8 The IR spectra of **1** (a), **2** (b) and **3** (c).

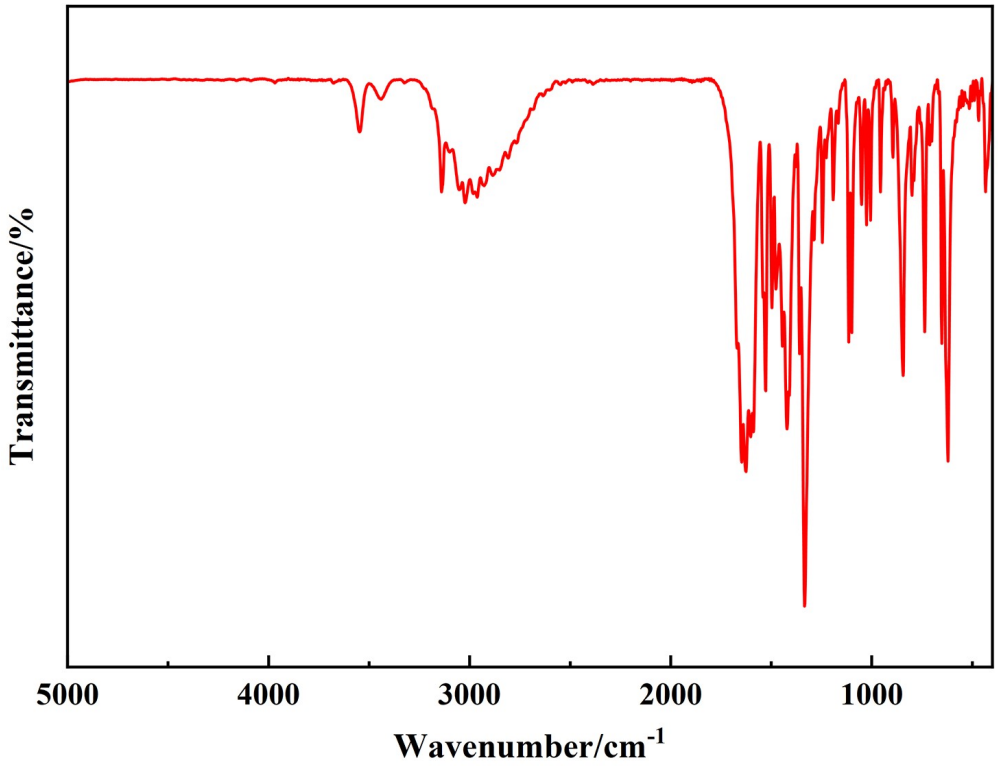

Fig. S9 The IR spectra of the L ligand.

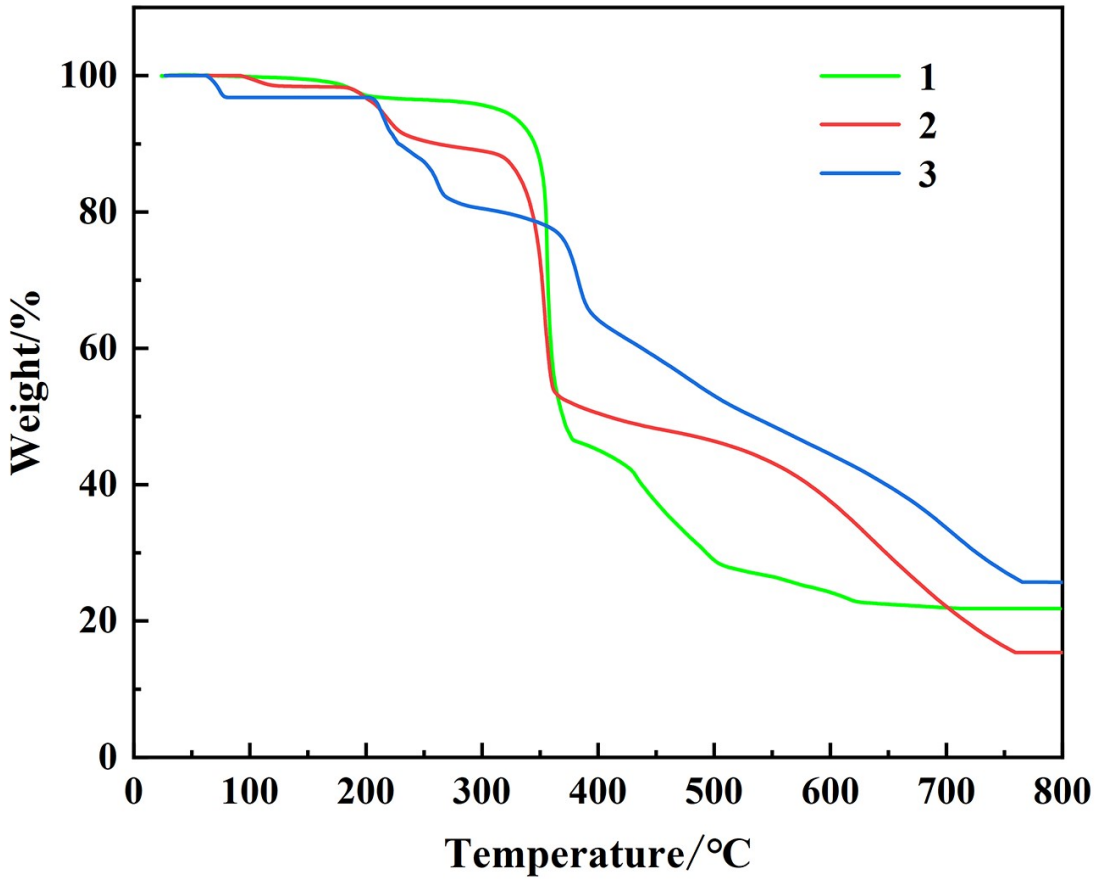

Fig. S10 TGA curves of **1**−**3**.

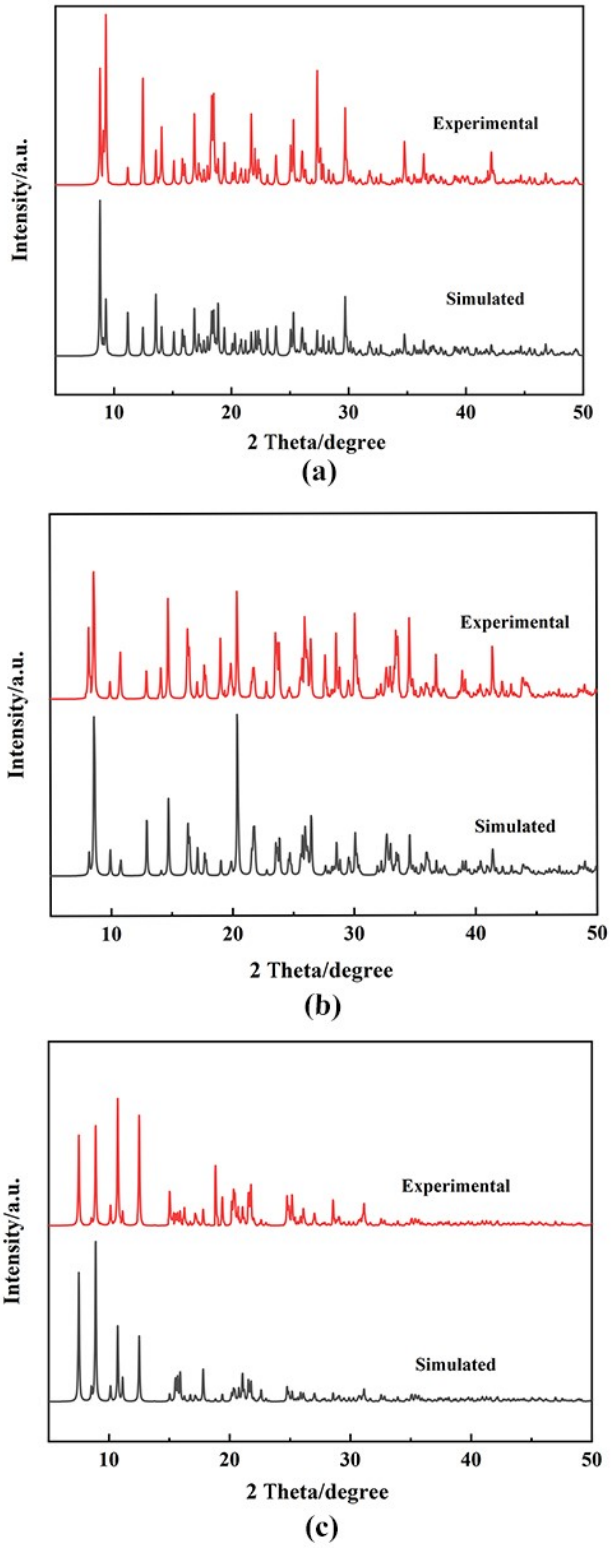

Fig. S11 Experimental and simulated PXRD patterns for **1** (a), **2** (b), and **3** (c).

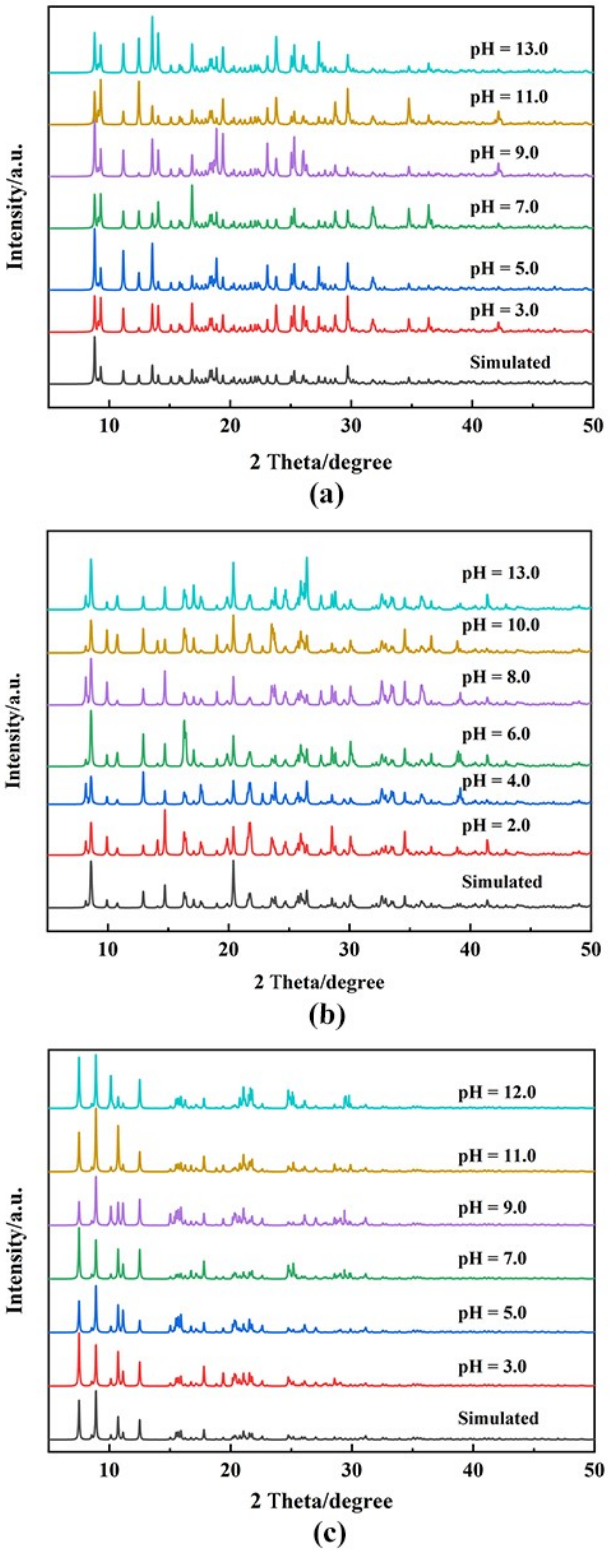

Fig. S12 PXRD patterns of **1** (a), **2** (b), and **3** (c) in different pH aqueous solutions.

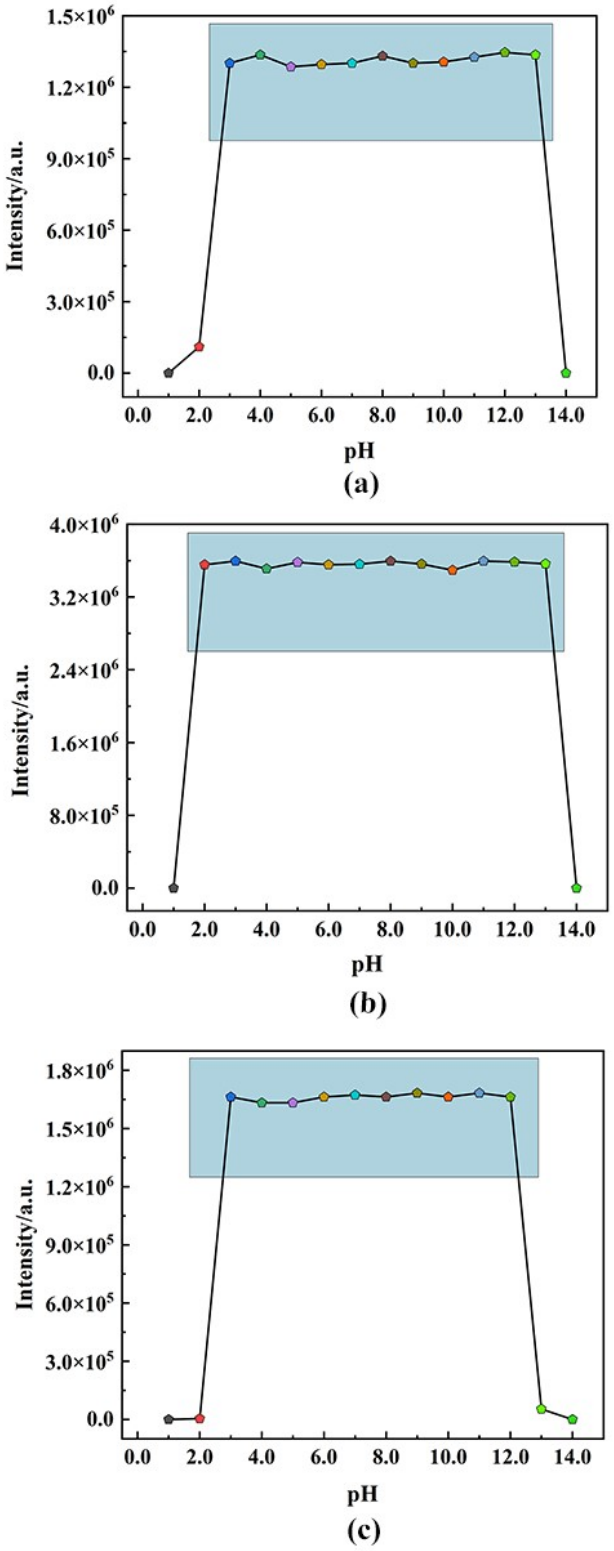

Fig. S13 The luminescence intensity of **1** (a), **2** (b), and **3** (c) in different pH aqueous solutions.

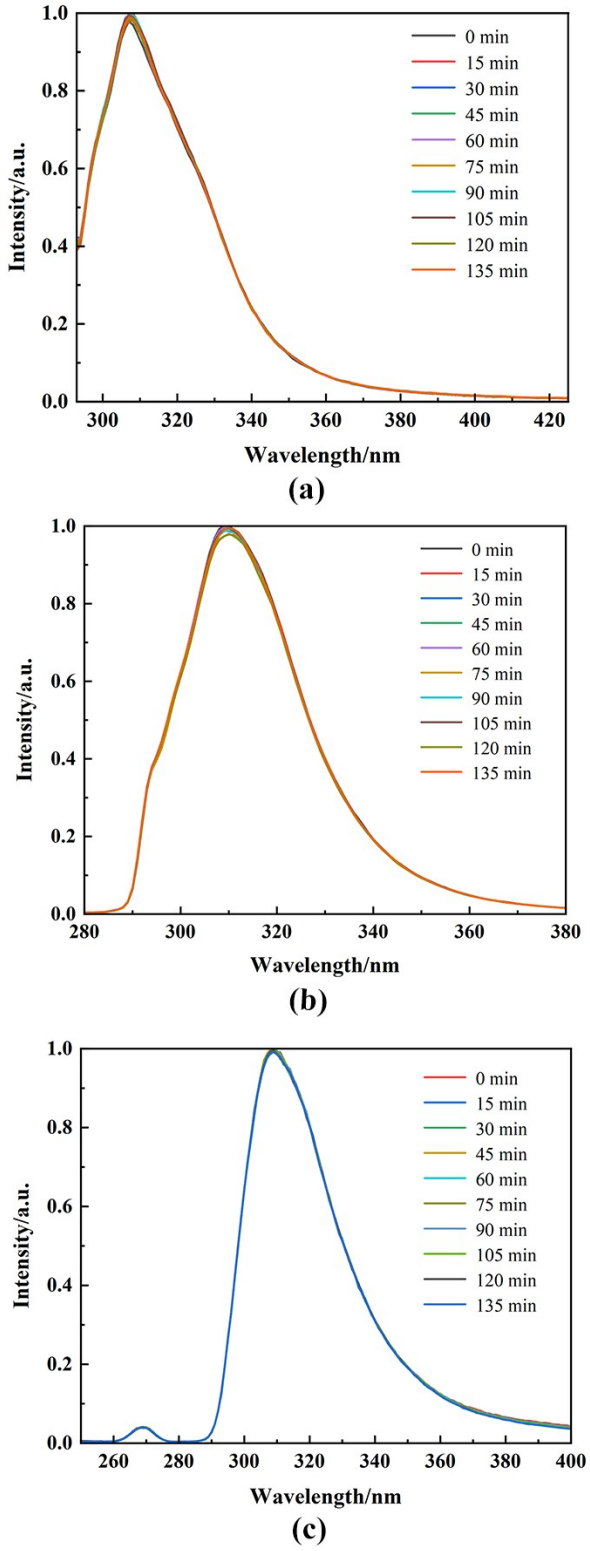

Fig. S14 Time-dependent emission spectra of **1** (a), **2** (b), and **3** (c) suspended in aqueous solutions.

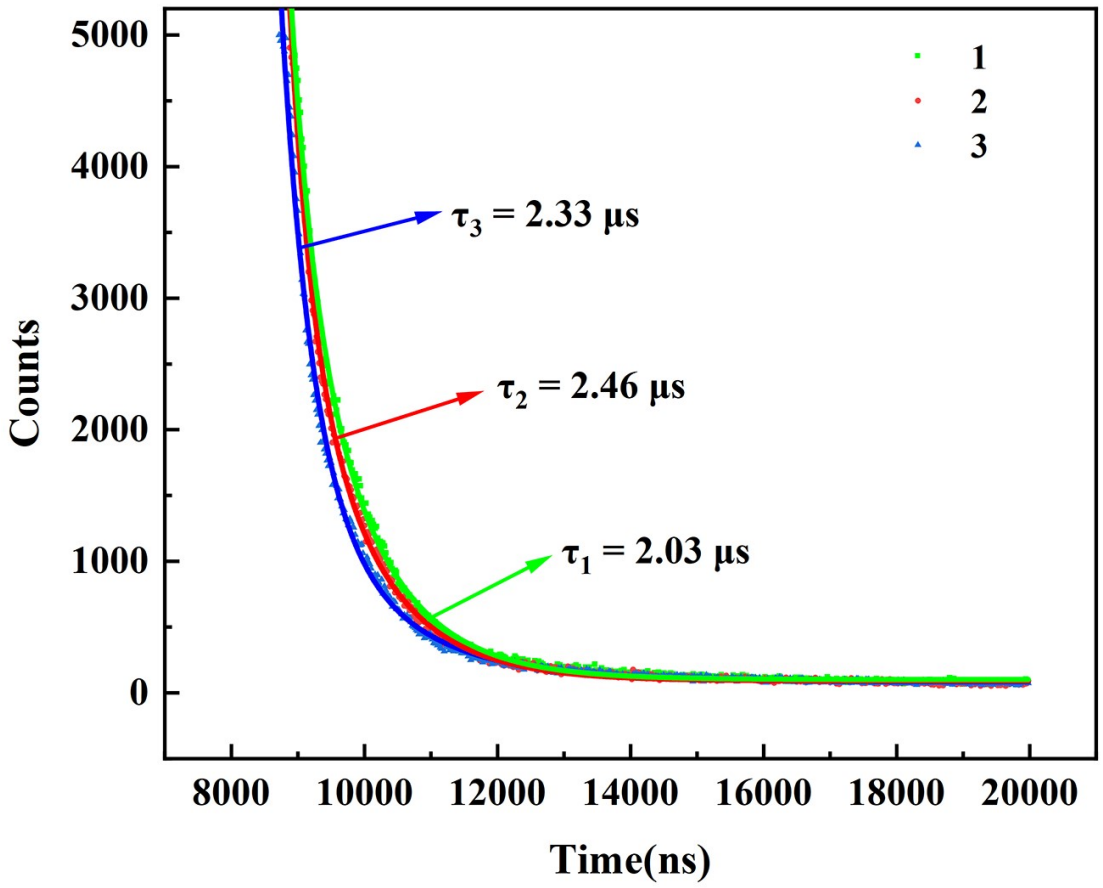

Fig. S15 Time-resolved luminescence spectra (symbols) with bi-exponential fit (solid lines) to the decay curves for **1**−**3**.

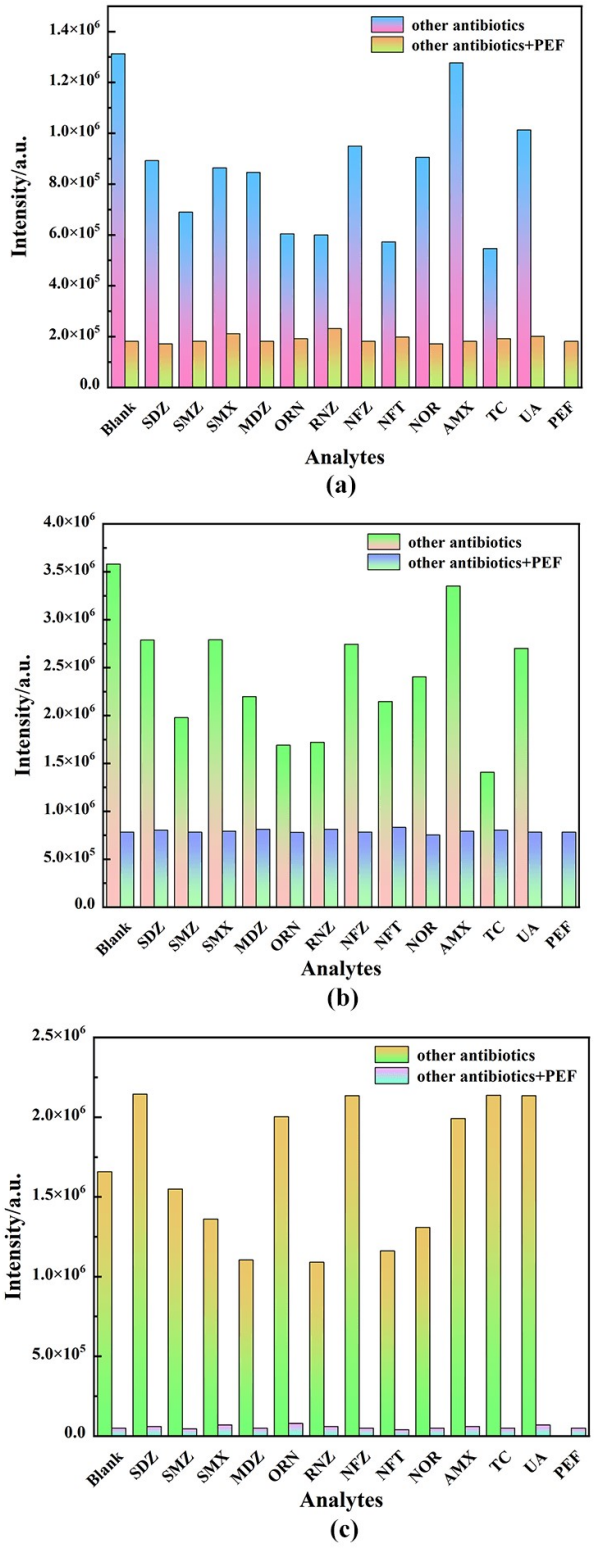

Fig. S16 Anti-interference experiments of **1** (a), **2** (b), and **3** (c) for PEF with other antibiotics.

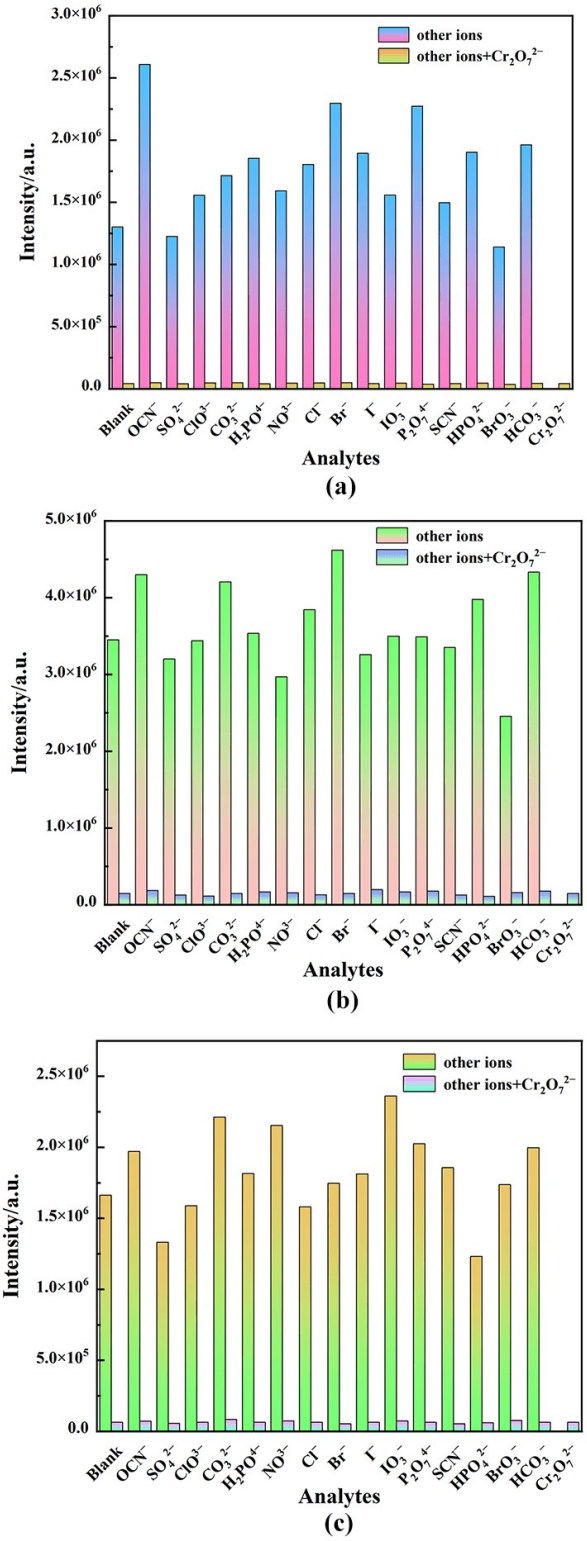

Fig. S17 Anti-interference experiment of $Cr_2O_7^{2-}$ ions in **1** (a), **2** (b), and **3** (c) to different metal ions.

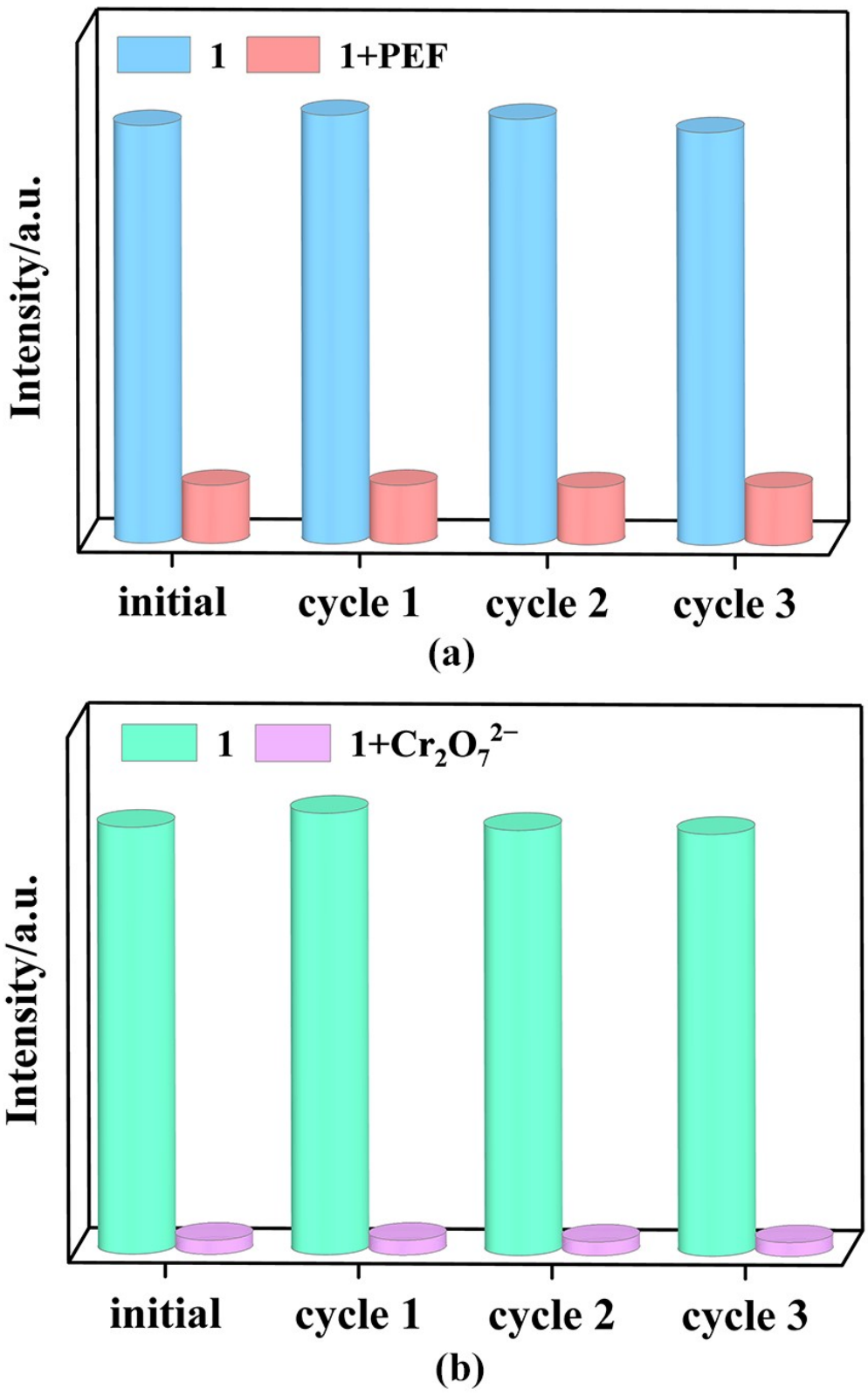

Fig. S18 Reversibility of **1** for the detection of PEF and $Cr_2O_7^{2-}$ ions.

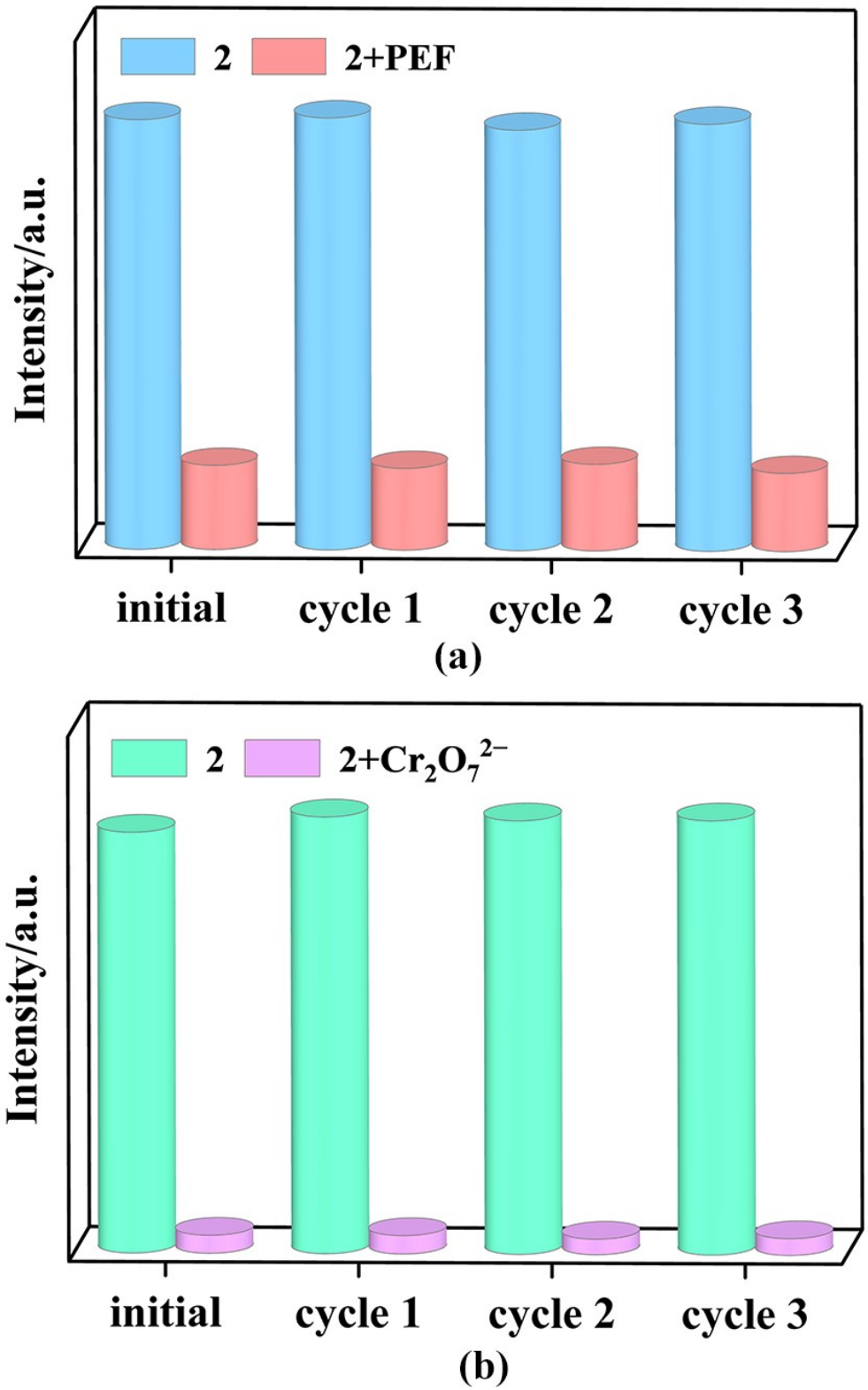

Fig. S19 Reversibility of **2** for the detection of PEF and $Cr_2O_7^{2-}$ ions.

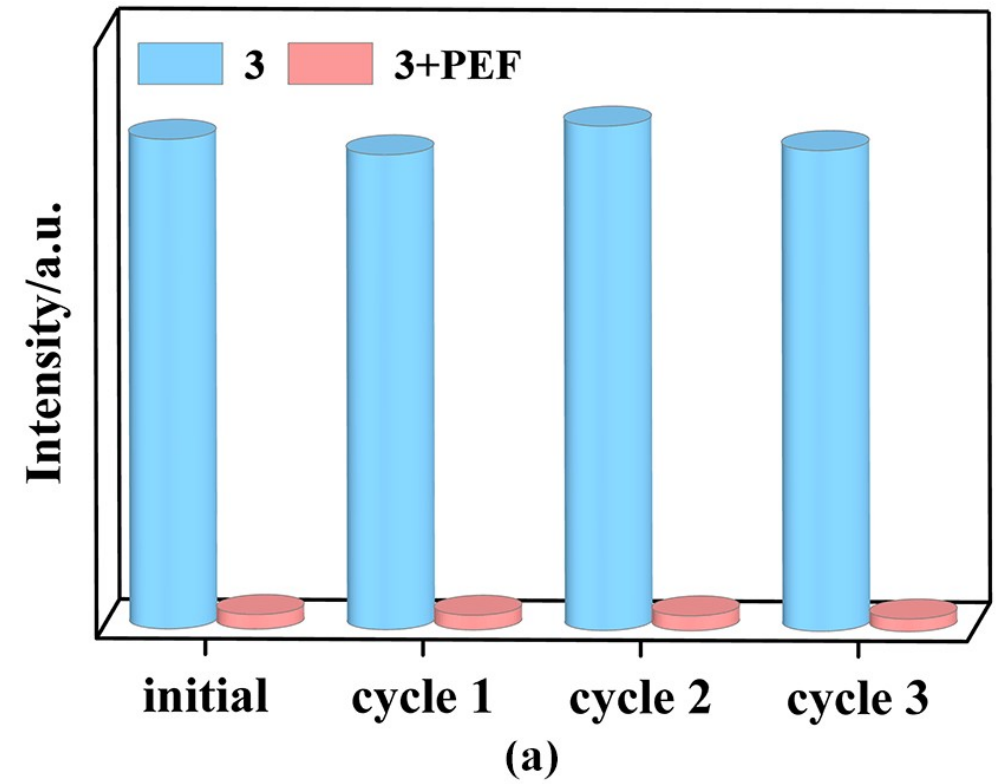

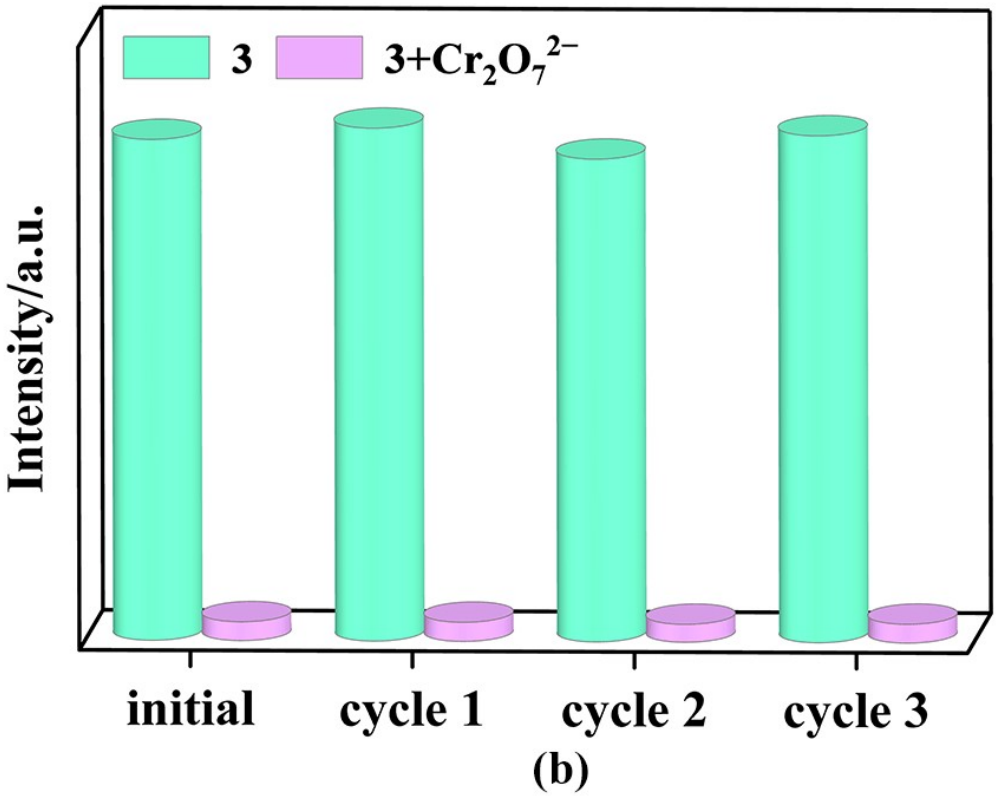

Fig. S20 Reversibility of **3** for the detection of PEF and $Cr_2O_7^{2-}$ ions.

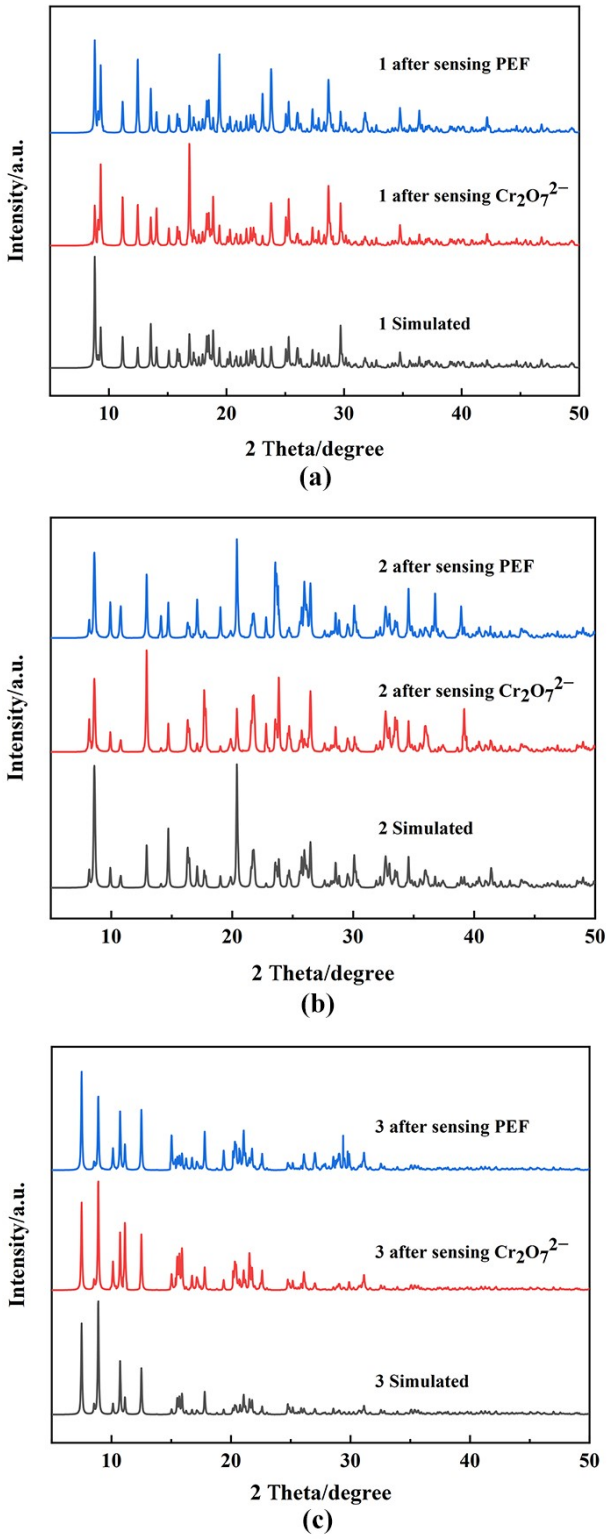

Fig. S21 PXRD patterns of **1** (a), **2** (b), and **3** (c) after sensing analyte.